Article

Assessing the Hazard of Flooding from Breaching of the Alacranes Dam in Villa Clara, Cuba

Victor Manuel Carvajal González [1], Carlos Lázaro Castillo García [2], Lisdelys González-Rodriguez [3,4,*], Luciana Silva [5] and Jorge Jiménez [2]

1   Facultad de Construcciones, Universidad Central "Marta Abreu" de Las Villas,
     Carretera a Camajuaní Km 9 1/2, Santa Clara 50100, Cuba; vicarvajal@uclv.cu
2   Facultad de Ingeniería, Universidad de Concepción, Concepción 4030000, Chile;
     carloscastillo2025@udec.cl (C.L.C.G.); jorgejimenez@udec.cl (J.J.)
3   Facultad de Ingeniería y Negocios, Universidad de Las Américas, Sede Concepción,
     Concepción 4030000, Chile
4   Centro de Modelación Ambiental y Dinámica de Sistemas (CEMADIS), Universidad de Las Américas,
     Santiago 7500000, Chile
5   Facultad de Ciencias Ambientales, Universidad de Concepción, Concepción 403000, Chile; lucisilva@udec.cl
*   Correspondence: lgonzalezr@udla.cl

Abstract

Flooding due to dam failures is a critical issue with significant impacts on human safety, infrastructure, and the environment. This study assessed the potential flood hazard that could be generated from breaching of the Alacranes dam in Villa Clara, Cuba. Thirteen reservoir breaching scenarios were simulated under several criteria for modeling the flood wave through the 2D Saint Venant equations using the Hydrologic Engineering Center's River Analysis System (HEC-RAS). A sensitivity analysis was performed on Manning's roughness coefficient, demonstrating a low variability of the model outputs for these events. The results show that, for all modeled scenarios, the terrain topography of the coastal plain expands the flood wave, reaching a maximum width of up to 105,057 km. The most critical scenario included a 350 m breach in just 0.67 h. Flood, velocity, and hazard maps were generated, identifying populated areas potentially affected by the flooding events. The reported depths, velocities, and maximum flows could pose extreme danger to infrastructure and populated areas downstream. These types of studies are crucial for both risk assessment and emergency planning in the event of a potential dam breach.

Keywords: dam failure; hydraulic modeling; HEC-RAS; hazard map; flooding event

1. Introduction

Floods caused by dam failure or dam breaching represent a hydrological phenomenon of great relevance due to their potential to generate flood peaks significantly greater than those caused by natural events such as intense rainfall [1]. Throughout history, dams have failed due to different events or loading conditions [2]. Generally, most documented dam and levee failures are often linked to exceedances of design water levels according to the United States Army Corps of Engineers [3]. In addition, the scientific community has identified other types of failures, such as piping and internal filtration in a dam's inner structure, which results in a piping process [4]. Although dam breaching flood hydrographs usually have lower values than those produced by exceeding the water level, they are significantly higher than the values generated by discharge through the spillway or the emergency flood drains [4].

Over the past 100 years, there have been around 200 dam failures, resulting in more than 30,000 deaths [2,5]. One example was the failure of the Vaiont Dam in Italy, where 2600 lives were lost [2]. Another recent dam failure event due to exceeding storage capacity occurred in Derna, Libya, where more than 11,000 people lost their lives [5].

Given the high hazard that dam failure poses to nearby communities, studies based on mathematical simulations [6] are often required for hazard assessment of new construction. These studies include an assessment of how the new construction would affect river flows, its banks, and floodplains [1,7]. According to Bellos et al. [8], dam breach analyses are divided into two submodels: (a) the dam breach submodel, which is responsible for producing the flood hydrograph, and (b) the hydrodynamic submodel, which uses the flood hydrograph to determine flood peaks and maximum water depths downstream of the dam.

Studies have developed equations to estimate the size of a dam breach or failure (width, slope, eroded volume, etc.), as well as failure time. These equations were derived from data obtained from earth dams, dams with impermeable cores (e.g., clay, concrete, etc.), and rockfill dams. They are not directly applicable to concrete dams or earth dams with concrete cores [3]. Notable works in this area include Froehlich David [9], and Froehlich David [10], which performed multiple linear regressions to develop an equation that predicts the peak discharge following an earth dam failure. In 2008, another study presented an improved mathematical expression based on 74 data points of dam failures (both piping and overtopping). The study characterized the phenomenon and analyzed the uncertainty in predicting peak flows and water levels by using Monte Carlo simulations [11]. Authors Xu and Zhang [12] have presented empirical equations to predict dam failure parameters based on 182 failure cases. Other proposed models include MacDonald and Langridge-Monopolis (1984) and Van Thun and Gillete (1990), which can be found in ref. [13]. Peramuna et al. [14] reviewed the techniques used in routing modeling of the flood. In addition, they explored the different one-dimensional hydrodynamic models (1D) and two-dimensional (2D) hydrodynamic models to simulate the propagation of the flood. USACE [7] explored advantages, disadvantages, and differences between these simulations and suggests 2D modeling for some cases, since it can produce better results than 1D modeling.

A well-known tool for flood analysis is the Hydrologic Engineering Center's River Analysis System (HEC-RAS) model. It has been used to analyze water flow in Socas et al. [15], and to determine floodplains, and design hydraulic engineering solutions such as dam breach studies [16–20]. In Albu et al. [16], HEC-RAS was used to model a dam breach in a mountainous area, highlighting the importance of topographic features in flood propagation. Meanwhile, Marangoz & Anilan [17] focused on simulating partial dam failures, demonstrating how different dam breaching configurations affect flood dynamics. Mao et al. [21] discuss a management system designed for dam-break hazard mapping using MIKE-21 in complex basin environments. It outlines methodologies for data integration and simulation of dam failure scenarios, which are crucial for generating hazard maps. The research emphasizes the importance of establishing a database for dam-break hazard mapping and spatializing hydrological calculations to create effective flood hazard maps. Ongdas et al. [18] applied HEC-RAS in an urban context, assessing the impact of dam failure in densely populated areas. These results helped to identify critical areas for the implementation of mitigation strategies. Another discussion highlights the use of 2D hydraulic models for producing flood hazard maps [22]. Pilotti et al. [19] explored the model's sensitivity to different hydraulic and terrain parameters, providing a framework to improve simulation accuracy and to reduce uncertainty in results.

Cuba has faced unique challenges in dam management due to its geography and tropical climate. According to the Cuban National Institute of Hydraulic Resources (INRH in Spanish), a total of 242 dams have been counted, 238 of which are earth dams, and more than 200 of which were built between 1960 and 1980 [23]. Published studies for Cuba to date focus solely on geotechnical and seismological aspects of earth dams [24–27]. Despite the documentation on the problems of Cuban's earth dams, studies on flood failure and catastrophic flow events are not well documented. There is a need to update methodologies and to provide helpful information to local authorities. The only guideline for calculating time and dam breaching parameters is the Cuban Standard NC 974 2013 [28]. However, this standard does not offer information on the outflow hydrograph, which is essential for assessing the magnitude of the impact of the failure over time. The absence of this information hinders the understanding of hazards involving these events, as well as the ability to prepare comprehensive strategies aimed at minimizing the impact of disasters. In addition, the impact of the phenomenon on a regional scale has not been quantified. Stucchi et al. [29] and Socas et al. [15] reported flooding events due to rainfall episodes; however, these conditions are not similar to dam failure events.

The primary goal of this study was to provide a comprehensive methodology for flood hazard assessment due to dam breaching. The method included a systematic, multi-scenario modeling framework that integrates empirical breach parameter estimation, sensitivity analysis of hydraulic roughness coefficients, and high-resolution 2D hydrodynamic modeling. This research introduces scientific novelty through three key contributions: (1) the first application of thirteen complementary breach models (including physical and empirical approaches) in order to quantify uncertainties in flood wave propagation for an earthen dam located in a tropical climate with complex coastal plain topography; (2) the identification of critical threshold conditions where breach geometry and formation time exponentially amplify flood extents in low-relief environments, as demonstrated by the derived Qmax-TFA power relationship (R^2 = 0.90); (3) the validation of Manning's roughness coefficient insensitivity for deep floodwaters (>6 m) through systematic parametric analysis, providing a methodological template for similar geomorphological settings; and (4) to provide spatially explicit information on flood dynamics that could be used by local authorities to prioritize mitigation actions, design evacuation routes, and plan emergency interventions. This research addresses the gap in regional-scale dam breaching risk assessment for Caribbean basin environments. In addition, this research establishes a replicable methodological framework for quantifying hydrodynamic uncertainties in low-lying coastal plains.

2. Materials and Methods

2.1. Procedure for Obtaining Maps for Reservoir Failure

Figure 1 presents the adapted methodological proposal. The Alacranes dam failure hazard maps were generated using the methodology described in Ferrari et al. [30], which follows four basic steps. In the first step, the study area was selected (Section 2.2), then a description of the terrain from the reservoir to the boundary conditions at the end of the model, and Manning's roughness coefficient values were obtained (Section 2.3). In the second step (Section 2.4), the failure mechanism (overtopping or piping) and the relationship between the initial hydraulic conditions (boundary conditions) were adopted. Thirteen modeling scenarios were developed: six for piping and seven for overtopping failure mechanisms. The third step (Section 2.5) was applied to the failure model and the flood routing model. To obtain the gap opening, the regression models of Froehlich David [10], Froehlich David [11], Van Thun and Gillete USACE [3], and Xu and Zhang [12] in their different variants were used along with the physical model (DL BREACH), which is integrated in the software [31]. The fourth step obtained the hazard map from using a 2D

flood routing model that included the topographic characteristics of the area (see Section 3). The depth, velocity, and hazard maps from breaching the Alacranes dam used the criteria reported by the State of New South Wales (Australia) and the Department of Planning Industry and Environment [32].
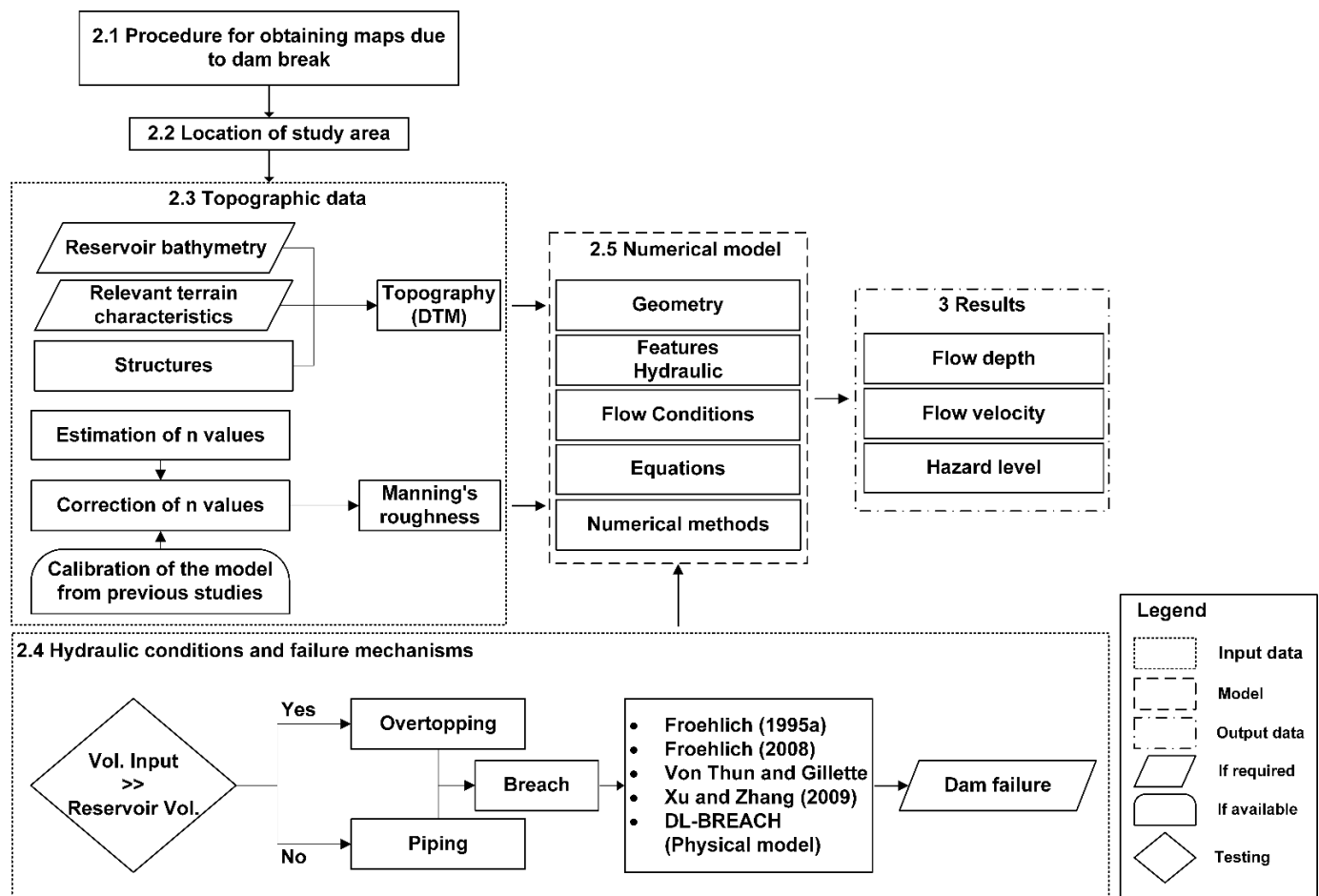
Figure 1. Flowchart for obtaining depth, velocity, and hazard maps for the Alacranes dam.

2.2. Location of Study Area

Figure 2a shows the location of the island of Cuba, highlighting the Villa Clara region represented in orange, while Figure 2b shows the Villa Clara province divided by cities (the city of Sagua la Grande City is highlighted in red). Figure 2c represents the Digital Terrain Model (DTM) around the Alacranes dam located 7 km southwest of the city of Sagua la Grande and 2 km west of the town of Sitiecito at coordinates E: 590,165, N: 324,733 (Lambert NAD 27 Cuba Norte conic projection). The dam was completed in 1972 and retains the waters of the Sagua La Grande River basin, which is the second largest basin in the country. The 15 km long and 5 km wide reservoir, through an extensive channel system, supplies the local chemical industry, as well as irrigates 196 km^2 of sugarcane in the Armonía area, 110 km^2 of pastures in Macún, and 150 km^2 in Sagua la Chica.
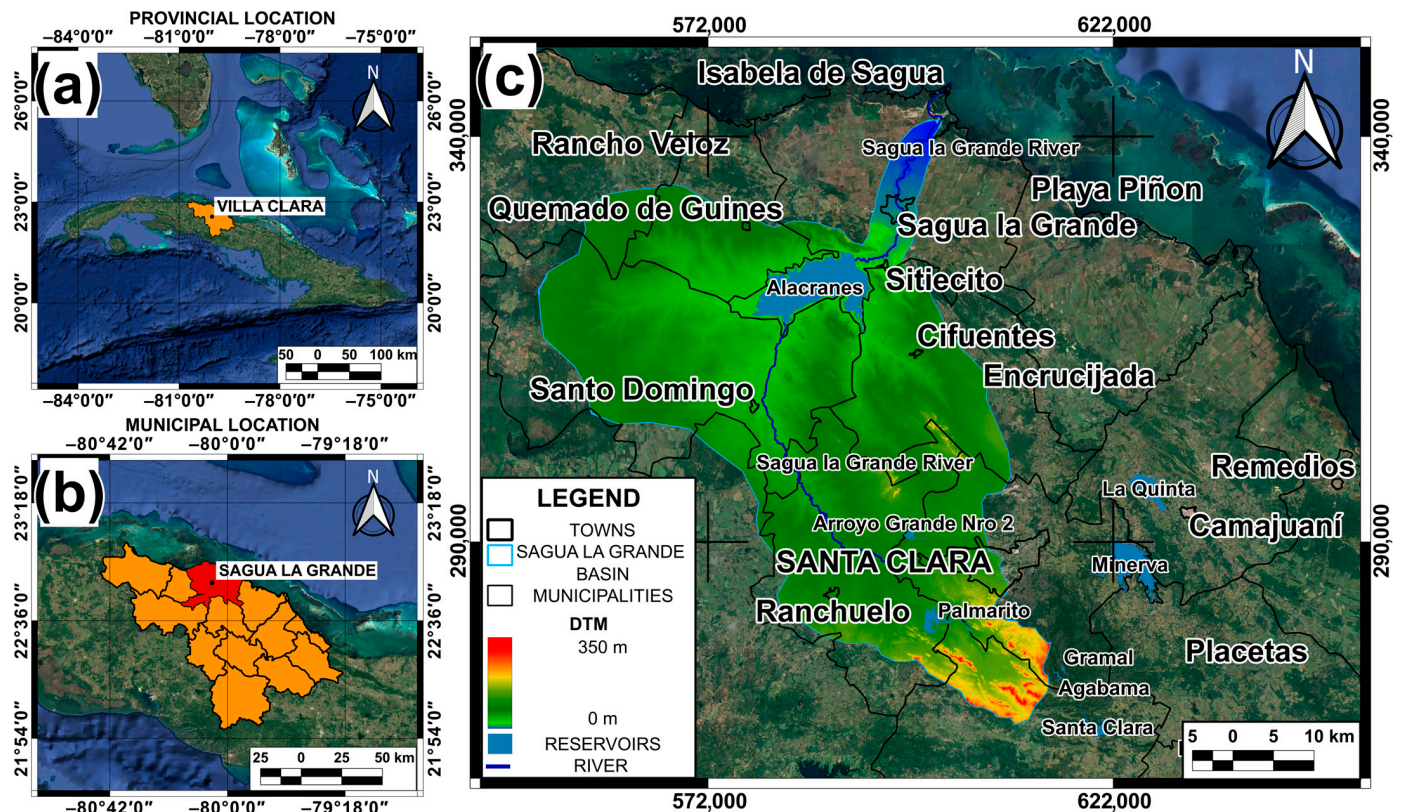
Figure 2. (**a**) Location of the island of Cuba, with the Villa Clara region represented in orange, (**b**) zoom of Villa Clara with the division by cities (the city of Sagua La Grande highlighted), (**c**) DTM around the Alacranes dam in the extension of the Sagua La Grande basin and nearby towns and other reservoirs.

The Alacranes Reservoir is the third largest in Cuba, with a storage volume of approximately 350 Mm^3. The reservoir has a composite section, with a central part (or core) of clay and outer rocky shoulders. Its maximum water level is 36 m.a.s.l (meter above sea level) and its normal water level is 32.32 m.a.s.l. The intake structure comprises a pressurized conduit, a control tower equipped with a radial (segment) gate, and a free-flowing discharge tunnel leading downstream. The guaranteed delivery is 325 Mm^3 per year. The spillway is a trench-type structure with an ogee-shaped (practical profile) crest, capable of discharging up to 2400 m^3/s through a rock-cut outlet channel carved in the rock until it joins the river. The city of Sagua La Grande is located downstream of the dam (Figure 3) and can be affected by severe flooding if the dam fails or if there is uncontrolled release of water. Additionally, small towns located along the river between Sagua la Grande and the coast may also be affected due to the flat topography near the river mouth. Potential hazards are influenced by both natural (e.g., earthquakes, storms, climate change) and human-related factors, such as aging infrastructure that may compromise dam safety. Understanding the interplay of these factors is crucial for effective disaster risk management and for developing strategies to mitigate the potential for life losses. Therefore, this location was selected for developing the province's first hazard map associated with a potential failure of the Alacranes Reservoir.
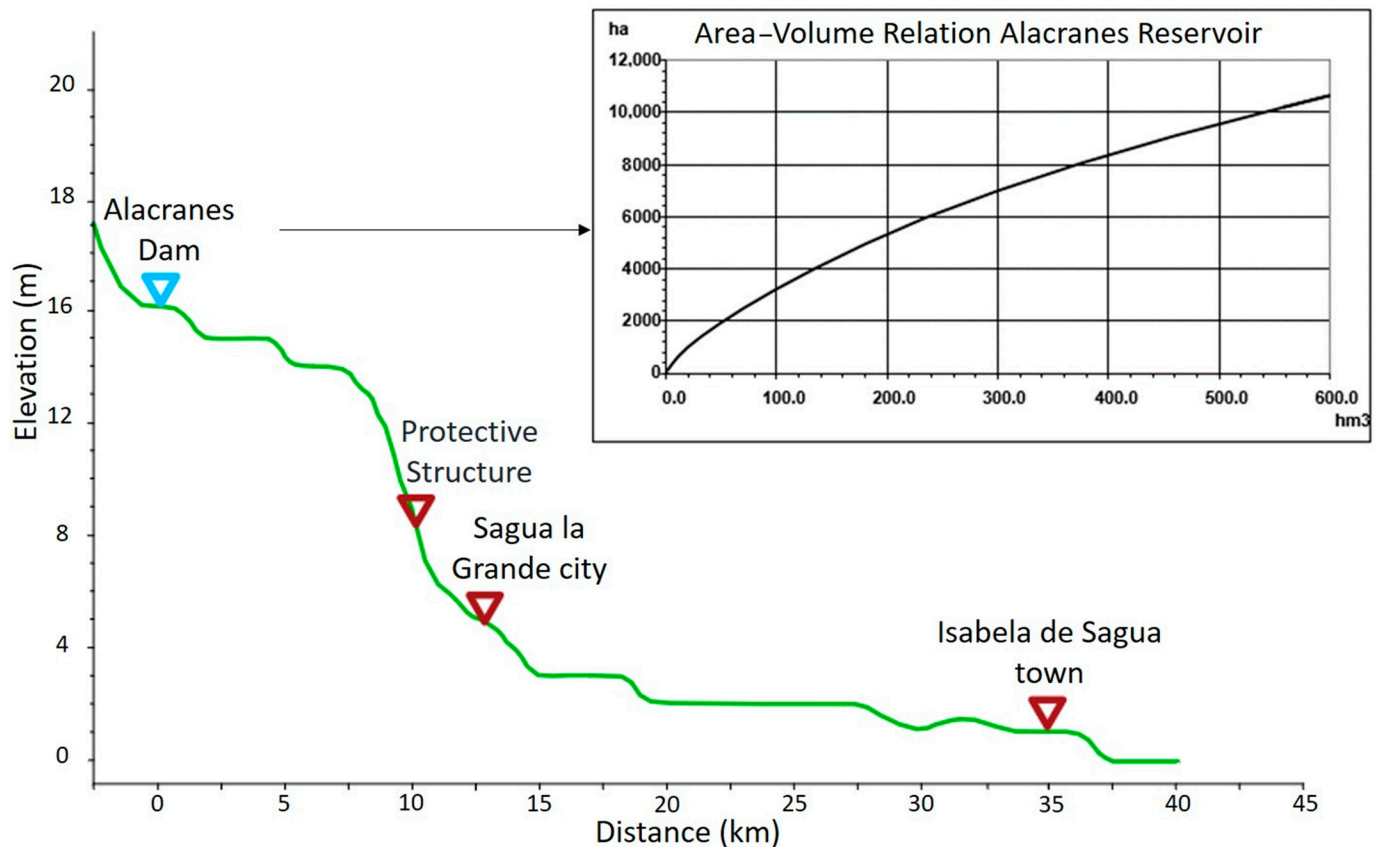
Figure 3. Longitudinal topographic profile and locations of points of interest from the Alacranes Reservoir to the mouth of the Sagua River in the town of Isabela de Sagua. The reservoir's area–volume curve is shown on the right.

2.3. Topographic Data

In order to describe the terrain elements that may interact with a flood caused by dam failure, the adoption of a high-resolution DTM is required [30,33]. For the Alacranes dam, the local DTM developed by the Cuban Geographical Studies Company (GEOCUBA) with a 12.5 m spatial resolution was used (See Figure S1). Figure 4 represents the local DTM with modifications extracted from the GEOCUBA database. The artificial contour lines within the Alacranes Reservoir based on height–volume curves are observed, allowing an approximate knowledge of the spatial variation of the bottom. This methodology is recommended by USACE [3], which explains that in case detailed bathymetric data are not available and a complete unsteady flow path is still desired, the cross-section data can be modified to match the published height–volume curve of the reservoir.

The local DTM included those man-made structures present in the area. Among these structures were the so-called "Puertas de Sagua," which consist of two dikes perpendicular to the river, forming a control section (see Figure 3) that allows approximately half of the spillway's maximum flow to be diverted to the coastal plain. These dikes, as indicated by a topographic survey, have been assessed as being in poor condition. In this study, this topographic survey was used to replicate the configuration of these dikes within the DTM, thus respecting their current condition as indicated by recent topographic measurements.
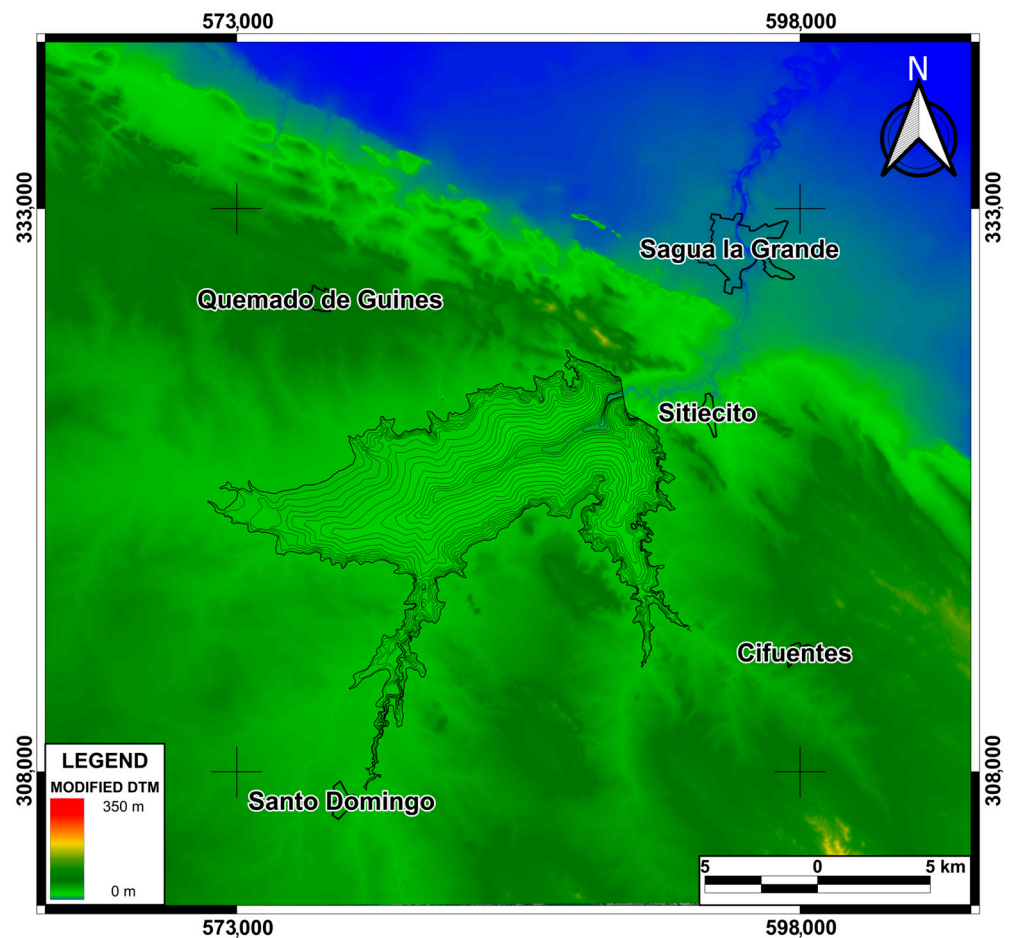
Figure 4. DTM modified digital elevation model of the Sagua La Grande basin highlighting the names of nearby towns.

To calibrate the Manning's roughness coefficient, a preliminary report of the flood footprint observed on the left bank of the river in the city of Sagua La Grande was used. This record was obtained from the reservoir's initial operation, which provided a valuable reference for adjusting the Manning's roughness coefficient value. The value estimated in Figure 5a corresponds to a spillway overflow event (1100 m^3/s), used to calibrate the model for routine flood behavior. This calibration does not apply to dam breach scenarios, as no historical breach data exist to validate such extreme events. To calibrate the Manning's roughness coefficient, three main steps were followed using Arcement and Schneider [34] and Te Chow and Saldarriaga [35], and include the procedures of Socas et al. [15], Kiwanuka et al. [36], and Mohamed et al. [37].

First, initial roughness values were obtained, as represented in Figure 5b, which covers an overview of the study area. Then, modeling was performed for a flow rate of 1100 m^3/s, comparing the results with the actual curve (Figure 5a) until reaching a maximum of R^2 = 0.82, visible in Figure 5c, which focuses on the city. Finally, the Manning's roughness coefficient was adjusted over the entire area, as presented in Figure 5d. The calibrated values, between the horizontal and vertical positions of the curve in Figure 5a and the curve modeled in Figure 5b, although specific to the channel and floodplain with an event of 1100 m^3/s, can be extrapolated to the entire area due to the similarity of both topographic and natural characteristics. The results after adjustments remained within the range specified by Arcement and Schneider [34].
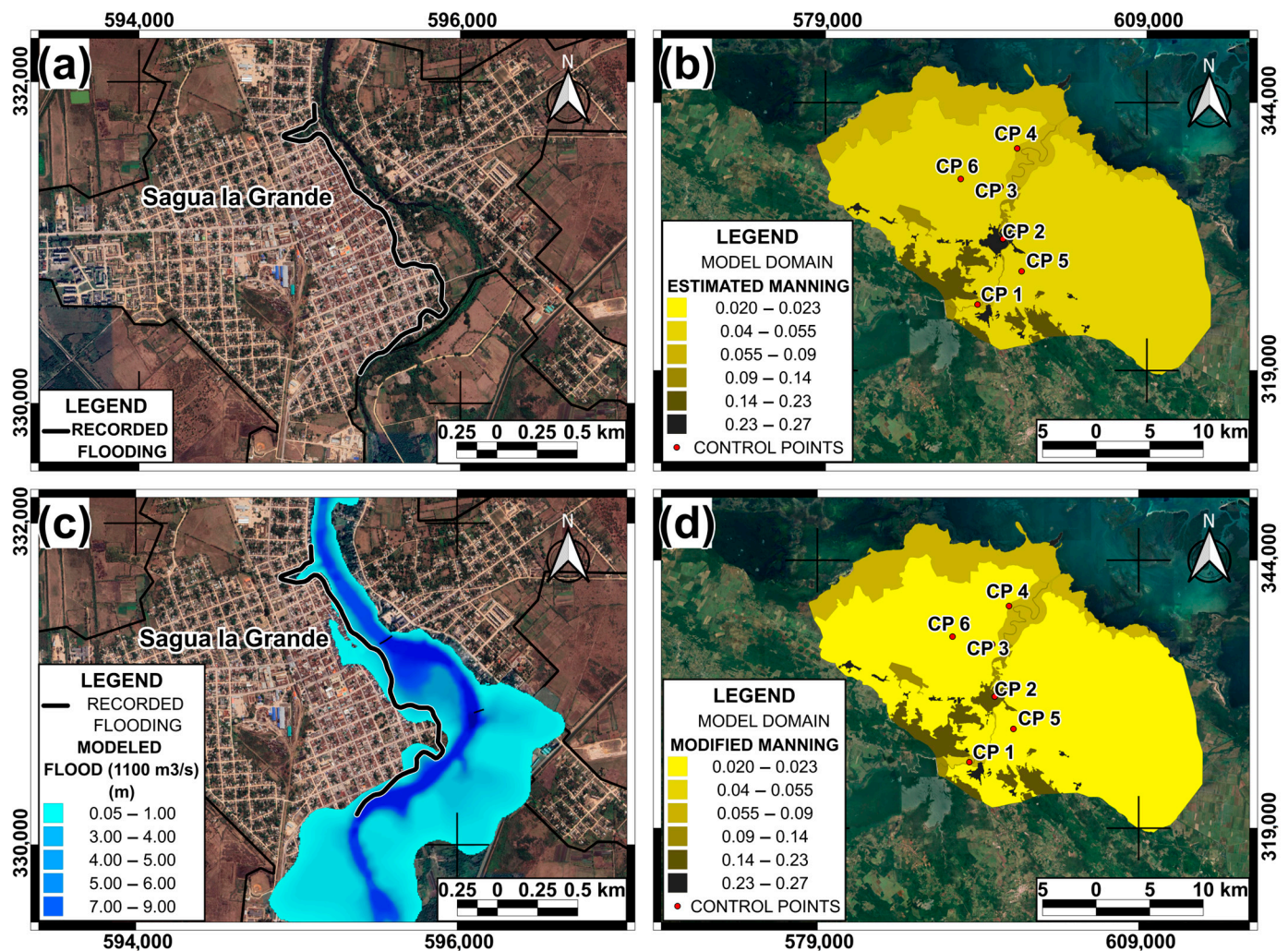
Figure 5. Representation of (**a**) water footprint, (**b**) estimated Manning's roughness coefficient, (**c**) modeled flood, and (**d**) modified Manning's roughness coefficient. The different control points (CP) are represented in red circles.

To estimate the initial peak discharge of 10,000 m^3/s as a mean approximation, the envelope equations were used as described in USACE [3]. Although this value was not used in the final model, it allowed for a sensitivity analysis of the roughness coefficient of the study area, using the control points (CP) represented by red circles (Figure 5b,d). Six control points were located at Sagua Highway Bridge (CP 1, E: 593,187, N: 325,162); El Triunfo Bridge (CP 2, E: 595,557, N: 331,276); plain near Isabela de Sagua (CP 3, E: 595,327, N: 336,136); coastal Plain (CP 4, E: 596,889, N: 339,727); coastal plain (CP 5, E: 597,301, N: 328,262); and coastal plain (CP 6, E: 591,616, N: 336,873).

Table 1 shows that for a range of ±20% of Manning's roughness coefficient, the flow velocity and depth values vary by less than 20% (see Table S1). This indicates that although the Manning's roughness coefficient is critical for flood routing, for large discharges, its influence is not significant when the water depth exceeds 6 m.

Table 1. Variation of depth and velocity under a sensitivity analysis for Manning's roughness coefficients.

Point Name	Modified Manning's Coefficient	0 Variation Manning's Roughness Coefficient		−20% Variation Manning's Roughness Coefficient		+20% Variation Manning's Roughness Coefficient	
		Depth (m)	Velocity (m/s)	Depth (m)	Velocity (m/s)	Depth (m)	Velocity (m/s)
CP1	0.074	8.41	1.35	7.95	1.57	8.82	1.21
CP2	0.091	9.37	2.28	9.15	2.76	9.55	1.99
CP3	0.029	0.20	0.21	0.17	0.22	0.23	0.2
CP4	0.056	0.52	0.36	0.45	0.41	0.57	0.31
CP5	0.029	0.69	1.04	0.51	1.05	0.85	1.00
CP6	0.029	0.24	0.39	0.20	0.43	0.27	0.36

2.4. Hydraulic Conditions and Failure Mechanisms

In order to simulate the dam breaching scenarios due to overtopping and piping failure, simplified boundary conditions were defined. In the case of overtopping failure, the reservoir level was raised by simulating a flood that raised the water level to the crest, roughly representing an inflow hydrograph at the reservoir's tail. In the case of piping failure, the normal water level was maintained, depending solely on internal factors within the dam wall. Given the proximity to the mouth, a downstream sea level of 0 m was established (the use of high and low tides or waves was not considered because they do not occur frequently in that area), allowing for an initial simulation of the flood propagation. To explore a wide range of conditions in the event of an infrastructure failure, 13 different scenarios were modeled. Table 2 shows the types of breach scenarios analyzed and their formulation. The characteristics of each scenario, such as the location and dimensions of the breach, were defined according to Froehlich David [9,11], Von Thun and Gillete [3], and Xu and Zhang [12]. These empirical formulations allowed for estimating parameters of the development of a breach, such as its final length, propagation speed, and shape, based on attributes of the levee or dam involved, such as its height, length, and material.

The empirical models selected for this study [3,9,11,12] were chosen based on their applicability to earthfill and rockfill dams, which are similar in type and characteristics to the Alacranes dam. Froehlich's models are widely used for estimating breach outflow and dimensions, particularly for dams with erodible materials. Von Thun and Gillette's formulations provide specific equations for breach geometry and formation time, while Xu and Zhang's multiparameter nonlinear regression model incorporates both dam attributes and failure modes, enhancing its predictive capability. These models, combined with the physical DL BREACH model, ensure a comprehensive representation of potential failure scenarios.

Table 2. Modeling scenarios for the Alacranes dam failure.

Scenarios	Formulation	Type of Dam Failure
Scenario 1	Froehlich David [9]	
Scenario 2	Froehlich David [11]	
Scenario 3	Von Thun and Gillette (1990) A *	
Scenario 4	Von Thun and Gillette (1990) B *	Overtopping
Scenario 5	Von Thun and Gillette (1990) C *	
Scenario 6	Xu and Zhang [12]	

Table 2. *Cont.*

Scenarios	Formulation	Type of Dam Failure
Scenario 7	Froehlich David [9]	
Scenario 8	Froehlich David [11]	
Scenario 9	Von Thun and Gillette (1990) A *	
Scenario 10	Von Thun and Gillette (1990) B *	Piping
Scenario 11	Von Thun and Gillette (1990) C *	
Scenario 12	Xu and Zhang [12]	
Scenario 13	HEC RAS Physical model [30]	Overtopping

* According to USACE [3], the Von Thun and Gillette breach formation time equations are presented for both erosion-resistant and easily erodible dams. The original publication of both authors suggests that these limits be considered as upper limit and lower limit (A and C, respectively), while B is an intermediate value of erosion resistance.

The classification of hazard levels was based on the NSW and DPIE [32] criteria, considering the depth and velocity of the water at the assessment point. In this way, it was possible to develop hazard maps for one of the studied scenarios, following methodologies from recent dam failure studies, which proposed a comprehensive approach that combines 2D hydraulic modeling with HEC-RAS and multicriteria assessment of failure scenarios [30,38]. Similar to Paşa et al. [38], this study prioritized the generation of flood and hazard maps through simulations that consider key parameters such as breach formation time, breach geometry, and initial hydraulic conditions. However, unlike the approach applied to buttress and earth dams in Turkey, this study adapted empirical breach formation models to the context of Cuban earth dams. This included the unique topographic features of the Villa Clara coastal plain and local Manning's roughness coefficient conditions. Additionally, the analysis was extended to 13 scenarios to evaluate both overtopping and piping failures, replicating the methodological approach employed by Paşa et al. [38] in the analysis of multiple failure criteria. The scenario that presented the most critical results was selected.

A color scale was used for the hazard maps, ranging from blue (low hazard) to red (extreme hazard), with four intermediate classifications that allow for an understanding of the magnitude of the hazard on a large scale. The areas identified as "blind spots" in the two-dimensional hydraulic simulation within the flood hazard map were assigned as "low hazard." The model was not able to calculate hydraulic parameters in these areas due to their size and dispersion at very shallow depths. However, the absence of flood hazards, even in the form of stagnant pools of water, cannot be ruled out since that can be areas where water would naturally tend to accumulate. Although the limitations of a two-dimensional model do not allow for an accurate representation of these behaviors, it was prudent to consider the degree of hazard under these circumstances. For the preparation of this study, the assessment of different hydraulic variables at the control points was proposed, such as the total flooded area (TFA), the maximum water depth (MWD), the maximum water velocity (MWV), the flood arrival time (FAT), the reservoir evacuation time (RET), the total time of flood (TTF), and the average water velocity (AWV).

2.5. Numerical Model

The Navier–Stokes equations describe fluid motion in three dimensions. However, in the context of channel and flood modeling, further simplifications are required. A simplified set of equations are the shallow water (SW) equations, which applies when certain conditions are assumed: the flow is incompressible, with uniform density, and pressure is considered hydrostatic. Another assumption is that the vertical length scale is much smaller than the horizontal length scales. As a consequence of these assumptions, the

vertical velocity is small, and the pressure is hydrostatic [3]. Furthermore, the original Navier–Stokes equations are averaged using the Reynolds number to approximate turbulent motion by eddy viscosity [3]. To improve simulation time, a coarse underlying mesh was used, within which finer topographic details can be extracted [16]. HEC-RAS software (version 6.3.0), developed by the United States Army Corps of Engineers (USACE), was used. The software was designed to solve both the full 2D Saint-Venant equation and the 2D diffusion wave equations. This analysis represents a shallow water model, with the diffusion wave approximation of the shallow water equations (Equations (1) and (2)) specified below [3]:

$$\frac{\partial H}{\partial t} - \nabla \cdot \beta \nabla H + q = 0 \tag{1}$$

$$\text{where } \beta = \frac{(R(H))^{5/3}}{n|\nabla H|^{1/2}} \tag{2}$$

where H is the water surface elevation, t is time, the differential operator ∇ is a vector of two-dimensional partial derivative operators given by $\nabla = (\partial/\partial x, \partial/\partial y)$, β is the momentum coefficient, ∇H represents the gradient of the water surface elevation, q represents a lateral flow term, R is the hydraulic radius, and n is the Manning's roughness coefficient.

For the simulation, all data were imported into HEC-RAS and converted to the Hierarchical Data Format (HDF). Due to the large size of the study area, the model included an unstructured 45 m × 45 m grid on the plain and a smaller grid on the river channel, composed of a total of 314,426 cells downstream of the reservoir, while the dam was modeled as a spillway. This captured all the details of the study area while also ensuring the computational efficiency of the model. In order to design the dam within the HEC-RAS environment, it was necessary to enter the different dimensional parameters required in the module. As indicated in [16], the grid size is directly related to the accuracy of the results when simulating flows. With a high-resolution DEM available, preliminary tests were performed to identify the appropriate cell size. Initially, a 75 m × 75 m mesh was tested and then progressively reduced to 25 m × 25 m. It was found that a 45 m × 45 m mesh was the inflection point where the error for the overall volume did not decrease significantly and instead, the computational time began to increase significantly, as shown in Figure 6.
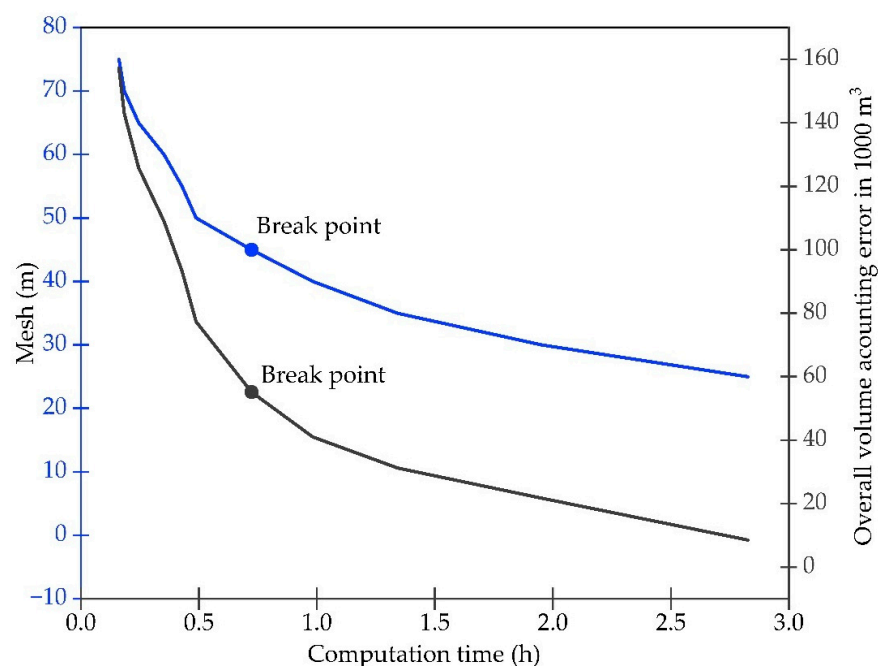
Figure 6. Variation in mesh size and volume accounting error with respect to computational time.

3. Results

Table 3 shows the results related to dam failure formation, such as average breach width, time to failure, total duration of each simulation, error in estimating the total generated volume, and maximum peak flow during the breach. It was observed that the widths of the breach base vary significantly, from 85 m to 350 m. In the case of the overtopping scenarios, the average breach width value calculated in NC 974-2013 [39] for the Alacranes dam was 250 m, being within the range of values obtained. The breach development times ranged from 0.40 h to 11.88 h, while in the NC standard, the time obtained was 6.2 h. The overall volume accounting error (the difference between input and output volumes in the simulation) was generally low, with values from 0.004% to 2.35%. Maximum flows (Q_{max}) showed wide variability, with values ranging from 6860 m^3/s to 35,726 m^3/s. For all scenarios, the Courant coefficient remained constant between 1 and 0.45. These results reinforce the conclusion of including several types of analyses in these studies.

Table 3. Computational, mathematical, and hydraulic parameters of the breach formation at the Alacranes dam outlet.

Scenarios	Type of Failures	Breach Bottom Width (m)	Breach Development Time (h)	Running Time			Overall Volume Accounting Error		Q_{max} (m^3/s)	Courant Coefficient	
				h	min	s	1000 m^3	%		Max	Min
Scenario 1	Overtopping	345.0	11.88	32	26	2	21,303.00	2.352	19,505	1	0.45
Scenario 2		311.0	10.34	19	3	8	94.44	0.011	19,893		
Scenario 3		100.4	0.50	26	32	12	71.60	0.008	13,480		
Scenario 4		100.4	1.00	27	13	14	76.85	0.009	12,983		
Scenario 5		95.0	0.65	13	14	9	34.07	0.004	15,184		
Scenario 6		207.0	11.71	31	51	59	89.96	0.010	15,553		
Scenario 7	Piping	171.0	6.69	23	50	14	93.14	0.020	12,423		
Scenario 8		166.0	6.02	15	17	37	85.00	0.018	11,291		
Scenario 9		90.0	0.40	19	55	27	55.38	0.012	6860		
Scenario 10		90.0	1.20	20	15	7	50.58	0.011	7064		
Scenario 11		85.0	0.57	18	58	40	59.86	0.013	8122		
Scenario 12		109.0	9.70	26	46	36	66.49	0.014	8297		
Scenario 13	Overtopping	350.0	0.67	31	29	40	22,928.00	2.531	35,726		

After running the simulation for the 13 potential dam failure scenarios, the most relevant parameters were extracted in order to emphasize the comparison between scenarios. These parameters included (a) TFA (total flooding area), (b) MWD (maximum water depth) at Sagua Road Bridge (CP1), (c) MWV (maximum water velocity) at Sagua Road Bridge (CP1), (d) FAT (flood arrival time) from the time the breach occurs until the flood peak reaches El Triunfo Bridge (CP2) and enters the floodplain downstream to Sagua La Grande, (e) RET (reservoir evacuation time), (f) the total time of flooding the city of Sagua La Grande (TTF), and (g) AWV (average water velocity) at El Triunfo Bridge (Table 4).

The results of the comparative analysis between the different dam failure scenarios indicated that the total flooded area varies considerably between scenarios, with the HEC-RAS physical model (Scenario 13) showing the largest affected area with 604.6 km^2, while Von Thun and Gillette (1990) A* (Scenario 9) from piping presented the smallest flooded area with 501.7 km^2. This shows the differences in methodologies and their impact on the magnitude of the flooded areas. Likewise, the maximum water depth in CP1 varied

significantly with the HEC-RAS physical model reaching 12.47 m, in contrast to the Von Thun and Gillette (1990) B* from piping failure that reports 8.58 m (Scenario 10). These values indicated the potential severity of the flooding event depending on the scenario considered. The maximum water velocity and flood arrival time also showed a wide variability of FAT between 1.33 h and 3.33 h. This parameter is crucial for determining emergency response strategies to save human lives.

Table 4. Key parameters extracted from modeling different dam failure scenarios.

Scenarios	Type of Failures	TFA (km^2)	MWD (CP1) (m)	MWV (CP1) (m/s)	FAT (CP2) (h)	RET (h)	TTF (h)	AWV (CP2) (m/s)
Scenario 1	Overtopping	595.7	10.76	3.46	1.67	40.00	26.66	2.57
Scenario 2		594.1	10.80	3.42	1.67	34.00	29.00	2.50
Scenario 3		562.1	9.73	3.60	1.58	49.50	64.75	2.63
Scenario 4		561.5	9.68	3.38	1.67	49.50	64.00	2.94
Scenario 5		567.9	9.79	3.60	1.33	52.00	38.00	3.07
Scenario 6		585.1	10.16	3.32	1.83	46.00	29.34	2.60
Scenario 7	Piping	556.6	9.57	3.22	3.00	36.00	23.67	2.29
Scenario 8		548.8	9.35	3.22	3.00	34.00	25.00	2.32
Scenario 9		501.7	8.48	3.31	2.67	49.50	34.66	2.74
Scenario 10		510.8	8.58	3.35	2.21	45.25	32.37	2.65
Scenario 11		519.9	8.69	3.40	1.75	41.00	30.08	2.56
Scenario 12		530.7	8.81	3.19	3.33	45.00	30.34	2.53
Scenario 13	Overtopping	604.6	12.47	5.55	1.33	43.67	23.34	3.21

In terms of average water velocity, the HEC-RAS model (Scenario 13) predicted values of 3.21 m/s, which has a significant destructive potential compared to the channel erosion velocities specified in Te Chow and Saldarriaga [35]. Overall, the consistency of results across different methods and models emphasized the importance of considering multiple approaches for an accurate and robust assessment of hazards of dam failure. The 13 scenarios analyzed revealed the exposure of buildings to backwater flooding. Figure 7 shows the saturation of the floodplain with floodwater, highlighting Scenario 13 as the most critical predicted condition by the HEC-RAS DL BREACH physical model. In addition, Figure 7 shows the city of Sagua La Grande, and several other towns located downstream of the dam. Both average and maximum depths were significant ($\leq$10 m) due to the greater destructive potential of flood waves in deeper water layers.

A relationship was found between the maximum break discharge variables Qmax and the total flooded area (TFA) with an R^2 of 0.90. Despite the limitations from establishing this relationship from only 13 scenarios, the equation that relates to both variables was

$$TFA = 173.9 Q_{max}^{0.1228} \tag{3}$$

When applying this relationship (potential equation), a flow rate ranging from 7000 m^3/s to 35,000 m^3/s could cause a total flooded area of 500 km^2 and 600 km^2. The most critical simulated scenario involved the formation of a 350 m gap in just 0.67 h (Scenario 13).
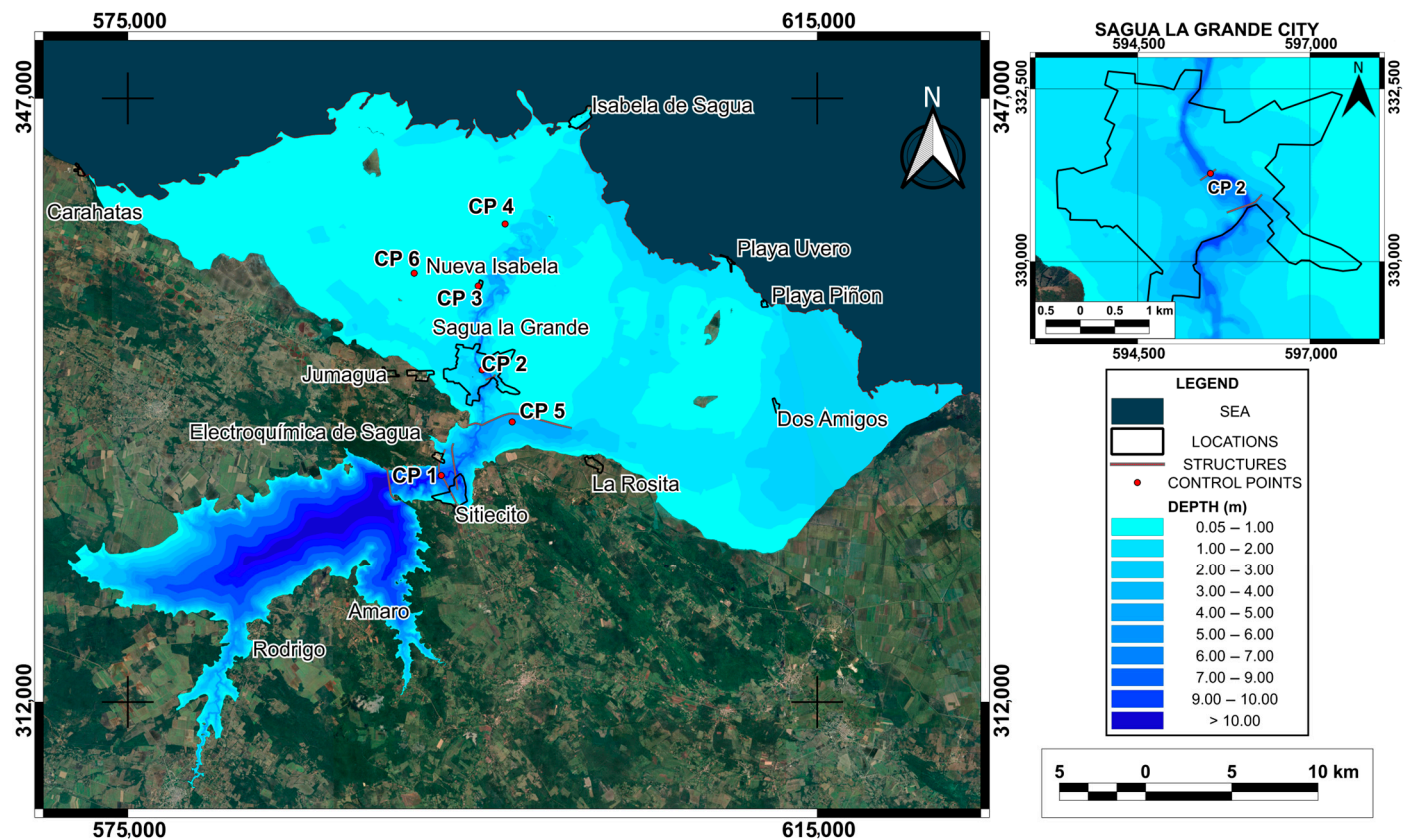
Figure 7. The Alacranes reservoir inundation zone for the event of a dam failure obtained for Scenario 13. To the right is the city of Sagua La Grande, with CP 2 marked in the center.

Figure 8 shows the velocity map obtained from the simulation of Scenario 13 (see Video S1). Water flow presented erosive velocities between 3 m/s and 5 m/s near structures such as bridges and protective dikes. The analysis at different CPs and at the flood protection structures known as Puertas de Sagua demonstrated that a dam breach greater than 10,000 m^3/s during the peak of the flood would overflow these protective structures. If the cause of a dam breaching was from a piping type of failure, there is a probability that the overflow threshold of these dikes could not be reached. However, if this threshold was exceeded, the flood would overflow these protective structures, and the coastline would be affected for an estimated length of 105 km. This would have an impact on several settlements and communities within the flood plain. It was preliminarily estimated that more than 49,000 people could be exposed to this hazard, affecting residents mainly in the city of Sagua La Grande (38,773 inhab.), as well as in the towns of Isabela de Sagua (2963 inhab.), Sitiecito (3871 inhab.), La Rosita (1635 inhab.), Nueva Isabela (980 inhab.), Dos Amigos (289 inhab.), Playa Uvero (200 inhab.), Playa Piñón (24 inhab.), and Caharatas (633 inhab.), among other villages and isolated individual homes (population data were obtained from the Cuban Collaborative Encyclopedia (EcuRed)) [40].

Figure 9 shows the hazard map developed for the study area with six different color levels defining red as extreme risk, yellow as severe hazard, light green as significant hazard, dark green as moderate hazard, light blue as caution, and dark blue as low hazard. The simulation revealed that, in the event of dam failure, the areas adjacent to the reservoir will experience significant flooding, affecting both critical infrastructure and local communities. The areas identified as being at extreme hazard are concentrated in the lower valley, where the city of Sagua La Grande, and towns such as Sitiecito, Nueva Isabela, Isabela de Sagua, Dos Amigos, Playa Piñon, and Playa Uvero are located. This finding is consistent

with previous studies indicating that topography directly influences water propagation following a structural failure of the dam.
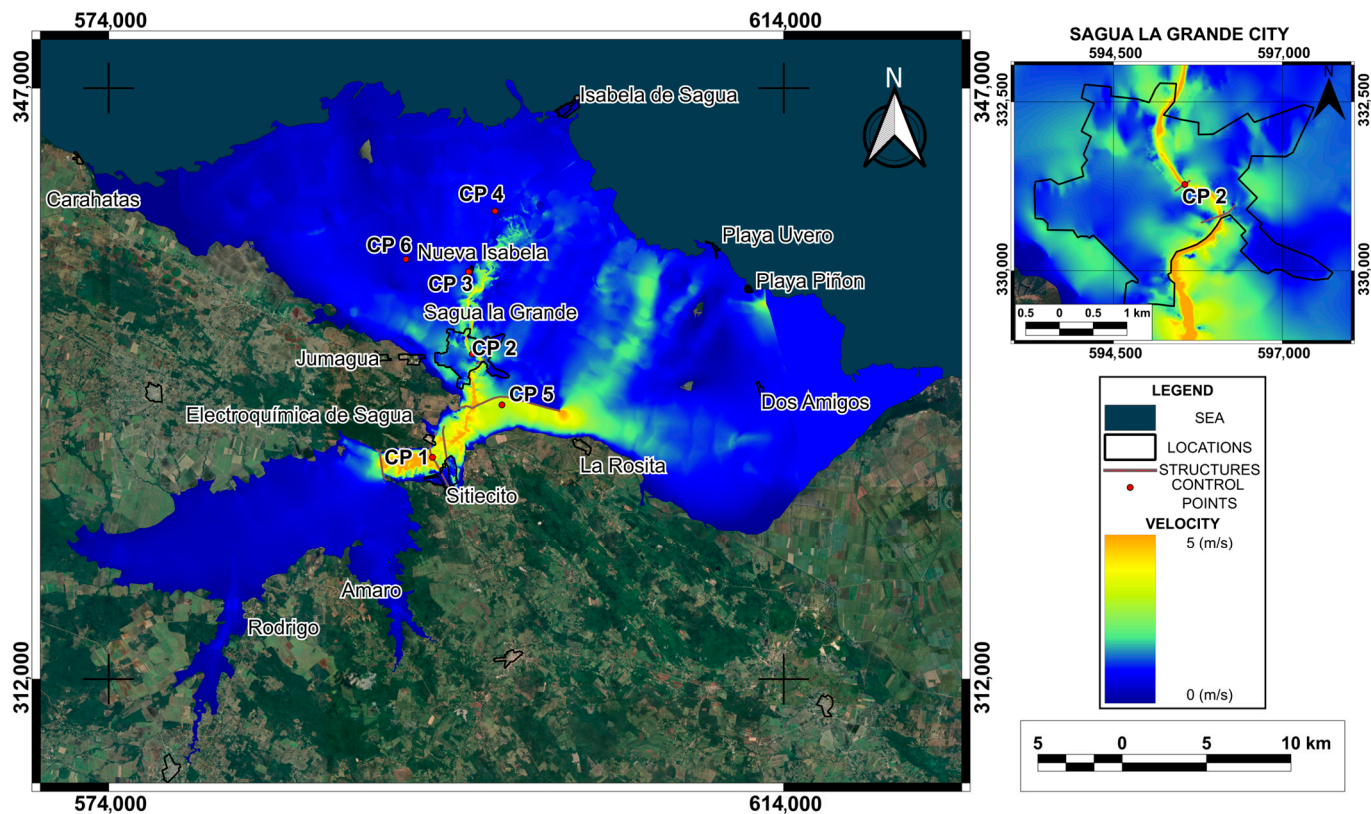
Figure 8. Map of simulated velocities at the time of greatest flood intensity obtained in Scenario 13. To the right is the city of Sagua La Grande, with CP 2 marked in the center.

It is important to emphasize that the city of Sagua La Grande, with a population of 38,733 inhabitants, would be one of the most affected areas as it is in the severe to extreme risk classification zone. Likewise, the town closest to the dam, Sitiecito, is in an area with this same hazard classification. Identifying these areas allows for prioritizing mitigation actions, such as creating evacuation routes and implementing early warning systems, which could reduce human loss and property damage.

Table 5 shows the percentage of urban areas near the reservoir along with their flood hazard classification. The city of Sagua La Grande has 91% of its area under a classification of severe to extreme flooding hazard, which was expected given its location downstream of the reservoir. Similarly, the town of Sitiecito has 63% of its area classified as extreme hazard for flooding. In the case of the town of Isabela de Sagua, since it is located on the coast, the hazard classification ranges from moderate to significant hazard. Other populated areas classified as caution and moderate hazard for flooding include La Rosita, Playa Uvero, Dos Amigos, and Playa Piñón. Even the town of Caharatas, located far from the dam breach, could be affected by the rising water level and humidity of the surrounding soil.
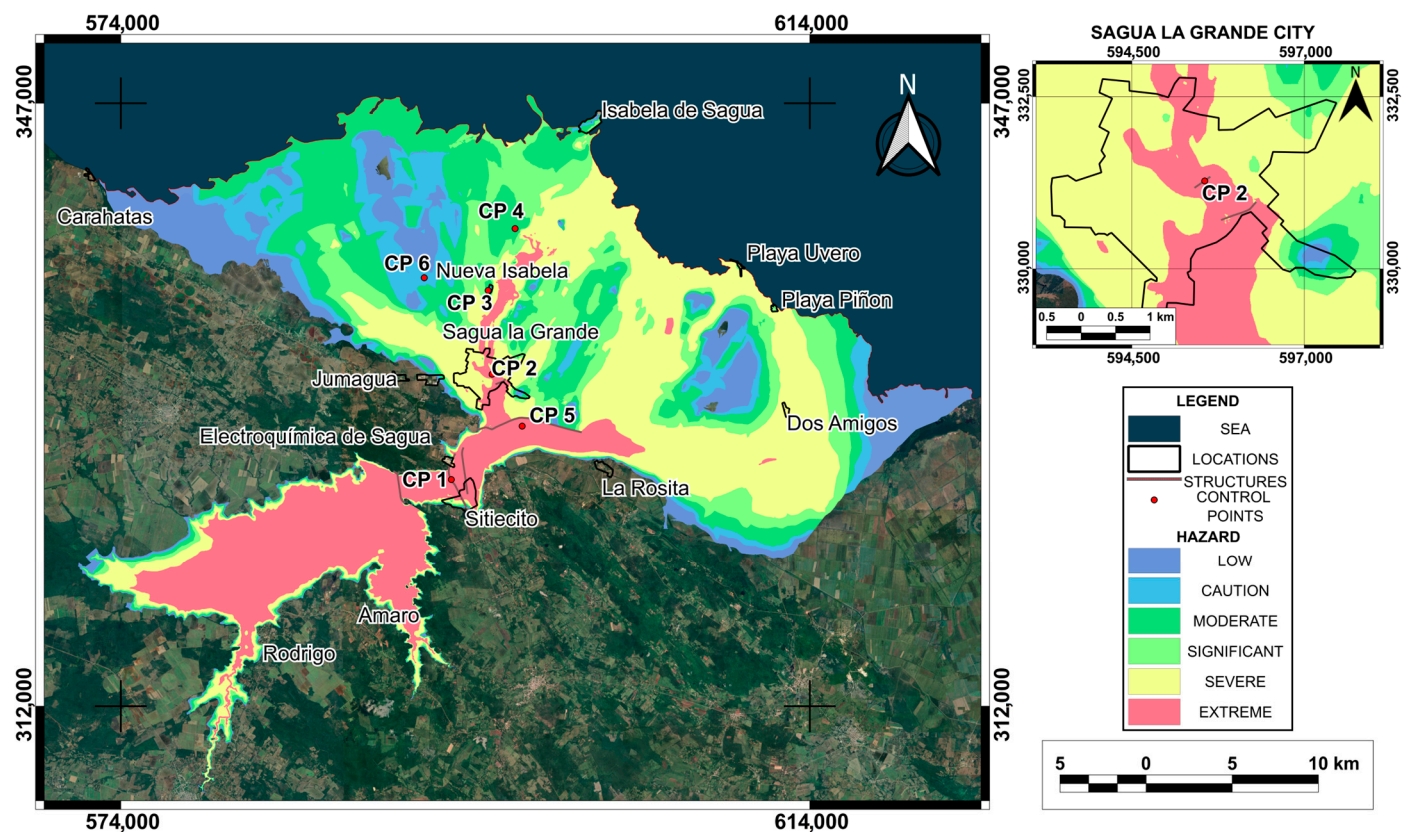
Figure 9. The Alacranes reservoir hazard map for Scenario 13 reservoir failure. To the right is the city of Sagua La Grande, with CP 2 marked in the center.

Table 5. Surface classification (in percentage) according to the level of flood hazard for the main populated areas affected by the Alacranes Reservoir failure.

City or Locality	Flood Hazard Ratings					
	Low	Caution	Moderate	Significant	Severe	Extreme
Sagua La Grande	1	1	3	5	61	30
Sitiecito	3	2	6	9	16	63
Isabela de Sagua	11	16	49	24	0	0
La Rosita [1]	0	0	0	0	50	50
Nueva Isabela	26	32	40	2	0	0
Dos Amigos	0	0	0	0	100	0
Playa Uvero	0	0	0	64	36	0
Playa Piñon	0	0	0	81	19	0
Caharatas [2]	100	0	0	0	0	0
Total affected area	9	10	27	18	30	6

[1] The town of La Rosita is located near areas of extreme hazard for flooding; therefore, the surface of this town was classified as 50% severe, 50% extreme hazard of flooding. [2] The town of Caharatas is not located within the flood hazard area. However, due to its proximity it was classified as low hazard for flooding.

4. Discussion

In this study, the methodology applied in Ferrari et al. [30] was adapted to the local conditions and data limitations of this particular study area in Cuba (lack of high-resolution topographic, bathymetry, and urban infrastructure data), starting with hydraulic analyses until obtaining the dam failure hazard map similar to those developed by Paşa et al. [38].

Using the hazard model reported by NSW and DPIE [32], the flood hazard in the area was analyzed and mapped for better understanding of the extent of the affected areas. The depth and velocity values produced by the simulations (Figures 7 and 8) can lead to significant riverbed erosion and landslides. Therefore, the river geometry can change during the flood event, as reported in [20,30,33,41]. Furthermore, mud and debris carried by the current can affect the dynamic conditions of the flow, which turns the water into a non-Newtonian fluid [3]. However, the results obtained do not take this into consideration; models with greater capacity and improvements in the implementation of roughness coefficients and/or non-Newtonian models are needed for future work.

Simulation results reported that dam failure affects roads and nearby populated areas such as the city of Sagua La Grande and nearby towns and communities such as Carahatas and Uvero and Isabela beaches in Sagua. Based on the use of rupture models, the most catastrophic event was determined to be the sudden failure of 350 m in 0.67 h (Scenario 13). Although the scenarios related to piping type dam failure were the least catastrophic, simulated flows up to 8000 m^3/s could produce an overtopping of the protective dike at the entrance to the city of Sagua La Grande (See Figure S2). These results are consistent with the events recorded by USACE [3], Fattorelli and Fernández [1], and Aureli, Maranzoni, and Petaccia [6], which suggested that piping events are less dangerous compared to overtopping dam failure.

For the study area, flood depth, flow, and flow velocity were determined to be as high as 12.47 m, 35,727 m^3/s, and 5.55 m/s, respectively, at the Sagua La Grande Highway Bridge (CP1) cross-section. Furthermore, results showed that flooding could reach a maximum flow of 35,727 m^3/s in 1.13 h at the same cross-section of the El Triunfo Bridge in the city of Sagua La Grande. It is worth noting that although Scenario 9 presents a significantly lower peak discharge (6860 m^3/s) compared to the most critical scenario (e.g., Scenario 13 with 35,726 m^3/s), the difference in total flooded area (TFA) is relatively small (~20%). This behavior can be attributed to the flat topography downstream of the dam, where floodwaters tend to spread laterally over large areas even under moderate flow conditions. In such environments, the total volume of released water and the duration of the event may have a greater influence on the extent of flooding than the maximum discharge alone.

When comparing the results presented in Table 6 with simulations conducted on dams of similar size and volume, the outcomes of Scenarios 1–12 align well with findings from previous studies [1–3]. For instance, the Oros dam in Brazil (35.4 m high, 700 Mm^3 storage capacity) generated a peak discharge of approximately 10,000 m^3/s under failure conditions. However, Scenario 13 yields significantly higher values compared to similar cases, highlighting how even smaller dams, such as the Malpasset dam in France, can experience increased peak discharges depending on reservoir volume and dam height. The observed differences among scenarios can be attributed to multiple factors, including dam geometry (height and crest length), stored water volume, data resolution, model accuracy, and local geographic features such as topography and land cover—factors that also influence variations in flood depth and velocity reported in other studies listed in Table 6. It is important to consider that simulations are based on hydraulic models that, although accurate, cannot predict all variables of water behavior in a real-life scenario [42]. Factors such as soil erosion and climate variability, as well as the presence of storm events, can influence the results. Therefore, follow-up studies are recommended to validate and adjust the model to combinations with intense rainfall, drought, or other initial boundary conditions, including breach parameters.

Table 6. Comparisons between this study and other studies of dam failure using HEC-RAS 2D model.

1	2	3	4	5	6	7	8	9	10	11
Alacranes	Cuba	21	350	O	350	604.6	10.8	3.5	35,726	This study
Ain Kouachia	Marruecos	22	11	O	88	3.2	20.3	8.0	9238	[20]
Yabous	Argelia	43	8	O	26	23.9	14.1	38.6	8767	[43]
Kibimba	Uganda	4.5	15	O	43	N/A	6.0	10.0	1935	[36]
Xe Namnoy	Laos	34	1050	O	N/A	46.0	9.5	12.0	8500	[41]
Chengbi River	China	70	1121	O	125	N/A	N/A	N/A	335,693	[33]
Wadi Al-Arab	Jordania	84	20	O	102	N/A	37.6	8.9	10,800	[44]
Wala	Jordania	54	25	O	133	N/A	43.0	17.1	12	[45]
Grand Ethiopian Renaissance (GERD)	Etiopía	145	74,000	O	200	N/A	50.0	7.0	325,928	[46]

1: Reservoir name, 2: Country, 3: Dam height (m), 4: Dam volume (Mm^3), 5: Overtopping (O: Overtopping), 6: Breach width (m), 7: Total flooding area (km^2), 8: Maximum water depth (m), 9: Maximum water velocity (m/s), 10: Peak discharge (m^3/s), 11: References, N/A: Not available.

A comparative analysis of the historical failures simulations listed in Table 6 provides essential context for our Alacranes dam results. For example, contrasting Alacranes with the Chengbi River dam highlights the influence of topography: although Alacranes' peak discharge (Qmax = 35,726 m^3/s) is an order of magnitude lower than Chengbi's (335,693 m^3/s), its position on a low-gradient coastal plain produces extensive lateral inundation spanning roughly 105 km of shoreline, versus the narrow, channelized flooding seen in steep basins. Likewise, comparing Alacranes to the GERD dam underscores the importance of proximity to population centers. A GERD breach would unleash a devastating Qmax of 325,928 m^3/s, yet the flood wave would take over three weeks to reach Khartoum, allowing ample time for emergency measures. By contrast, Alacranes sits only 7 km upstream of Sagua La Grande, placing nearly 49,000 people in immediate peril with minimal warning. Together, these comparisons demonstrate that dam-break hazard is governed not only by dam size or peak discharge but critically by local factors, chiefly the interplay between regional topography and settlement proximity.

Table 6 shows that Scenarios 1–12 produce flooded-area and peak-discharge figures in line with other 30–70 m high embankment dams (e.g., the Oros dam in Brazil, 35.4 m high, 700 Mm^3 storage, Qmax ≈ 10,000 m^3/s). In contrast, for Scenario 13, the Qmax ≈ 35,700 m^3/s markedly exceeds these values. This outlier reflects its exceptionally rapid breach formation (0.67 h), wide breach width (350 m), and the amplifying effect of a low-slope coastal plain. The remaining differences stem from variations in dam geometry (height, crest length), reservoir volume, data quality, model fidelity, and local geographic factors such as slope and land cover, all of which influence flood depth and velocity.

Some sources of uncertainty may affect the results: (1) Breach parameters (width and formation time) are based on empirical formulas with a typical variability of ±30% [43]. (2) The 12.5 m DTM lacks detailed bathymetry, which may bias water-level estimates in the floodplain. (3) Simplified hydraulic boundary conditions (constant spillway discharge of 1 100 m^3/s and fixed sea level) do not fully capture flood peaks or tidal variations. (4) The HEC-RAS 2D model uses the diffusive-wave approximation on a 45 m × 45 m mesh, without sediment transport or local inertia.

Although the Manning's coefficient sensitivity analysis showed <20% variation in depths and velocities and the overall volume error remained below 2.5%, we recommend that future work include Monte Carlo simulations [20] varying breach parameters, rough-

ness coefficients, and inflow rates, as well as incorporation of LIDAR bathymetry and the full Saint-Venant equations.

The use of web-based mapping tools such as DWR and SDSOD [47] to map reservoir breach flooding and flooding hazards in different locations across the state of California is an example of how scientific research can be integrated with state agencies responsible for public safety. Taking this approach would allow dynamic, high-resolution flood and risk maps to be developed for the Alacranes dam breach. These maps would provide local Cuban authorities with dynamic visualizations of flood risk, helping them to plan emergencies and prioritize protective measures.

5. Conclusions

The results of hazard maps for the Alacranes dam failure scenarios provided valuable information for hazard assessment and urban planning by identifying areas affected by potential flooding from a potential dam failure event. This could provide useful information to develop strategies to minimize the risks associated with dam failure. The simulation of multiple failure scenarios using different mathematical models showed significant variations in parameters such as flooded area, maximum depth, and maximum flow velocity, which depended on the type of structural failure of the dam.

According to the HEC-RAS physical model, the most critical failure scenario was Scenario 13, with the formation of a 350 m breach in just 0.67 h. The depth, velocity, and maximum discharge could be a significant hazard, endangering important infrastructure and several populated areas downstream of the dam. This study has important practical implications:

- Dam safety management: The hazard maps produced offer a valuable tool to assess the vulnerability of critical infrastructure and downstream communities. They can guide maintenance and reinforcement decisions for the Alacranes dam, thereby minimizing failure hazard. These results underscore the need to incorporate modeling studies into local hazard management policies, particularly in regions where hydraulic infrastructure dates back several decades and population exposure has grown significantly over time.

- Early warning system planning: The flood-wave arrival times identified in this study (some as short as less than two hours) are critical for designing realistic evacuation drills and improving coordination among institutions responsible for civil defense. These findings can inform the development of effective early warning protocols, ensuring communities receive timely alerts and have sufficient lead time to respond in the event of a dam failure.

- Regional risk mitigation: The findings pinpoint high-hazard zones in the city of Sagua La Grande, helping to prioritize investments in mitigation measures such as upgrades to drainage infrastructure and coastal defenses. By pinpointing the most hazardous zones (such as the urban area of Sagua La Grande) this analysis enables authorities to concentrate efforts on communities situated near aging, outdated earth dams where the risk is most imminent. For the first time, depth, velocity, and hazard maps have been produced for the areas downstream of the Alacranes dam in Cuba. However, the value of this study extends well beyond the local scale. By adapting robust methodologies to a data-limited context (e.g., in the absence of detailed bathymetry and high-resolution datasets), this work offers a replicable methodological framework. In practice, it demonstrates to authorities in other regions with similar constraints that it is feasible to develop precise, actionable risk-assessment tools. Consequently, rather than serving merely as a case study, this research provides a blueprint for strengthening emergency planning and resilience in vulnerable communities worldwide.

References

1. Fattorelli, S.; Fernández, P.C. *Diseño Hidrológico*, 2nd ed.; WASA-GN: Madrid, Spain, 2011; p. 379.
2. Costa, J.E. *Floods from Dam Failures*; 85-560; US. Geological Survey: Denver, CO, USA, 1985; pp. 9–11.
3. USACE. *HEC-RAS Hydraulic Reference Manual, 6.3*; US Army Corps of Engineers, Hydrologic Engineering Center: Davis, CA, USA, 2022.
4. Chaudhry, M.H.; Mays, L. *Computer Modeling of Free-Surface and Pressurized Flows*; Springer: Dordrecht, The Netherlands, 2012.
5. Mourad, Y. Searchers Look for More Than 10,000 Missing in Flooded Libyan City Where Death Toll Eclipsed 11,000. Available online: https://apnews.com/article/libya-floods-derna-storm-daniel-mass-graves-72307547f3e0ff4fbf715a7f64c69383 (accessed on 24 June 2024).
6. Aureli, F.; Maranzoni, A.; Petaccia, G. Review of Historical Dam-Break Events and Laboratory Tests on Real Topography for the Validation of Numerical Models. *Water* **2021**, *13*, 1968. [CrossRef]
7. USACE. *HEC-RAS 2D User's Manual, 6.3*; US Army Corps of Engineers, Hydrologic Engineering Center: Davis, CA, USA, 2022.
8. Bellos, V.; Tsakiris, V.K.; Kopsiaftis, G.; Tsakiris, G. Propagating Dam Breach Parametric Uncertainty in a River Reach Using the HEC-RAS Software. *Hydrology* **2020**, *7*, 72. [CrossRef]
9. Froehlich David, C. Peak Outflow from Breached Embankment Dam. *J. Water Resour. Plan. Manag.* **1995**, *121*, 90–97. [CrossRef]
10. Froehlich David, C. Embankment Dam Breach Parameters Revisited. In Proceedings of the First International Conference, Water Resource Engineering, Environmental and Water Resources Institute ASCE, Water Resources Engineering Proceedings, San Antonio, TX, USA, 14–18 August 1995.
11. Froehlich David, C. Embankment Dam Breach Parameters and Their Uncertainties. *J. Hydraul. Eng.* **2008**, *134*, 1708–1721. [CrossRef]
12. Xu, Y.; Zhang, L.M. Breaching Parameters for Earth and Rockfill Dams. *J. Geotech. Geoenviron. Eng.* **2009**, *135*, 1957–1970. [CrossRef]
13. USACE. *HEC-RAS User's Manual, 6.3*; US Army Corps of Engineers, Hydrologic Engineering Center: Davis, CA, USA, 2022.
14. Peramuna, P.D.P.O.; Neluwala, N.G.P.B.; Wijesundara, K.K.; DeSilva, S.; Venkatesan, S.; Dissanayake, P.B.R. Review on model development techniques for dam break flood wave propagation. *WIREs Water* **2024**, *11*, e1688. [CrossRef]
15. Socas, R.A.; González, M.A.; Marín, Y.R.; Castillo-García, C.L.; Jiménez, J.; da Silva, L.D.; González-Rodríguez, L. Simulating the Flood Limits of Urban Rivers Embedded in the Populated City of Santa Clara, Cuba. *Water* **2023**, *15*, 1805. [CrossRef]

16. Albu, L.-M.; Enea, A.; Iosub, M.; Breabăn, I.-G. Dam Breach Size Comparison for Flood Simulations. A HEC-RAS Based, GIS Approach for Drăcşani Lake, Sitna River, Romania. *Water* **2020**, *12*, 1090. [CrossRef]

17. Marangoz, H.O.; Anilan, T. Two-dimensional modeling of flood wave propagation in residential areas after a dam break with application of diffusive and dynamic wave approaches. *Nat. Hazards* **2022**, *110*, 429–449. [CrossRef]

18. Ongdas, N.; Akiyanova, F.; Karakulov, Y.; Muratbayeva, A.; Zinabdin, N. Application of HEC-RAS (2D) for Flood Hazard Maps Generation for Yesil (Ishim) River in Kazakhstan. *Water* **2020**, *12*, 2672. [CrossRef]

19. Pilotti, M.; Milanesi, L.; Bacchi, V.; Tomirotti, M.; Maranzoni, A. Dam-Break Wave Propagation in Alpine Valley with HEC-RAS 2D: Experimental Cancano Test Case. *J. Hydraul. Eng.* **2020**, *146*, 05020003. [CrossRef]

20. El Bilali, A.; Taleb, I.; Nafii, A.; Taleb, A. A practical probabilistic approach for simulating life loss in an urban area associated with a dam-break flood. *Int. J. Disaster Risk Reduct.* **2022**, *76*, 103011. [CrossRef]

21. Mao, J.; Wang, S.; Ni, J.; Xi, C.; Wang, J. Management System for Dam-Break Hazard Mapping in a Complex Basin Environment. *ISPRS Int. J. Geo-Inf.* **2017**, *6*, 162. [CrossRef]

22. Luke, A.; Mahajan, R.; Pilotti, M.; Ruebel, M.; Pasternack, G.; Faries, J.; Rosen, D.; Holmes, R.; Ahmad, M. Flood Hazard Maps Based on 2D Modeling. Available online: https://collaborate.asce.org/waterforum/discussion/flood-hazard-maps-based-on-2d-modeling-1 (accessed on 23 May 2017).

23. Morejón, S.M.; Haramboure, Y.G.; Rodríguez, O.Á. Comportamiento de las fallas de presas de materiales sueltos en Cuba. In Proceedings of the 18 Convención Científica de Ingeniería y Arquitectura, Palacio de las Convenciones de La Habana, La Habana, Cuba, 7–11 November 2016.

24. Flores Berenguer, I.; Castro Martínez, I.; García Tristá, J.; González Haramboure, Y. Influencia de la permeabilidad del suelo no saturado en los taludes de presas de tierra. *Ing. Hidráulica Y Ambient.* **2019**, *40*, 86–100.

25. Flores Berenguer, I.; García Tristá, J.; Haramboure, Y.G. Estabilidad de taludes durante un desembalse rápido en presas de tierra con suelos parcialmente saturados. *Ing. Y Desarro.* **2020**, *38*, 13–31. [CrossRef]

26. González Haramboure, Y.; Flores Berenguer, I.; García Tristá, J. Efecto de desembalse en la estabilidad de presas de tierra: Dos casos de estudio en Cuba. *Ing. Hidráulica Y Ambiental.* **2021**, *42*, 42–53.

27. Urquiza-López, Y.M.; Galbán-Rodríguez, L.; Nápoles-Fajardo, N.; Chuy-Rodríguez, T.J. El impacto de fenómenos geoambientales en cortinas de presas de tierra en Cuba. *Ciencia en su PC* **2017**, *1*, 56–69.

28. *NC 1239-2018*; Especificaciones Para el Diseño y Construcción de Alcantarillado Sanitario y Drenaje Pluvial Urbano. Oficina Nacional de Normalización (ONN): La Habana, Cuba, 2018.

29. Stucchi, L.; Bignami, D.F.; Bocchiola, D.; Del Curto, D.; Garzulino, A.; Rosso, R. Assessment of Climate-Driven Flood Risk and Adaptation Supporting the Conservation Management Plan of a Heritage Site. The National Art Schools of Cuba. *Climate* **2021**, *9*, 23. [CrossRef]

30. Ferrari, A.; Vacondio, R.; Mignosa, P. High-resolution 2D shallow water modelling of dam failure floods for emergency action plans. *J. Hydrol.* **2023**, *618*, 129192. [CrossRef]

31. Wu, W. Simplified Physically Based Model of Earthen Embankment Breaching. *J. Hydraul. Eng.* **2013**, *139*, 837–851. [CrossRef]

32. NSW; DPIE. *Flood Risk Management Committee Handbook: A Guide for Committee Members*; State of NSW and Department of Planning Industry and Environment: Parramatta, Australia, 2019.

33. Mo, C.; Shen, Y.; Lei, X.; Ban, H.; Ruan, Y.; Lai, S.; Cen, W.; Xing, Z. Simulation of one-dimensional dam-break flood routing based on HEC-RAS. *Front. Earth Sci.* **2023**, *10*, 1027788. [CrossRef]

34. Arcement, G.J.; Schneider, V.R. *Guide for Selecting Manning's Roughness Coefficients for Natural Channels and Flood Plains*; No. 2339; USGPO: Washington, DC, USA, 1989.

35. Te Chow, V.; Saldarriaga, J.G. *Hidráulica de Canales Abiertos*; McGraw-Hill: New York, NY, USA, 1994.

36. Kiwanuka, M.; Chelangat, C.; Mubialiwo, A.; Lay, F.J.; Mugisha, A.; Mbujje, W.J.; Mutanda, H.E. Dam breach analysis of Kibimba Dam in Uganda using HEC-RAS and HEC-GeoRAS. *Environ. Syst. Res.* **2023**, *12*, 31. [CrossRef]

37. Mohamed, M.J.; Karim, I.R.; Fattah, M.Y.; Al-Ansari, N. Modelling Flood Wave Propagation as a Result of Dam Piping Failure Using 2D-HEC-RAS. *Civ. Eng. J.* **2023**, *9*, 2503–2515. [CrossRef]

38. Paşa, Y.; Peker, İ.B.; Hacı, A.; Gülbaz, S. Dam failure analysis and flood disaster simulation under various scenarios. *Water Sci. Technol.* **2023**, *87*, 1214–1231. [CrossRef] [PubMed]

39. *NC 974-2013*; Presas, Diques de Protección, Canales y Obras Asociadas. Categorías Para Nuevos Proyectos o Para el Rediseño de Estructuras Existentes en un Escenario de Cambio Climático Cambiante. Oficina Nacional de Normalización (ONN): La Habana, Cuba, 2013.

40. WikiSysop. Localidades de Sagua la Grande, Quemado de Güines y Encrucijada. 2009. EcuRed. Sagua La Grande. Available online: https://www.ecured.cu/Sagua_la_Grande#Consejos_populares (accessed on 10 October 2024).

41. Latrubesse, E.M.; Park, E.; Sieh, K.; Dang, T.; Lin, Y.N.; Yun, S.-H. Dam failure and a catastrophic flood in the Mekong basin (Bolaven Plateau), southern Laos, 2018. *Geomorphology* **2020**, *362*, 107221. [CrossRef]

42. Chow, V.T.; Maidment, D.R.; Mays, L.W. *Hidrología Aplicada*; Suárez, M.E., Ed.; McGraw-Hill Interamericana: Bogotá, Colombia, 1994.

43. Gaagai, A.; Aouissi, H.A.; Krauklis, A.E.; Burlakovs, J.; Athamena, A.; Zekker, I.; Boudoukha, A.; Benaabidate, L.; Chenchouni, H. Modeling and Risk Analysis of Dam-Break Flooding in a Semi-Arid Montane Watershed: A Case Study of the Yabous Dam, Northeastern Algeria. *Water* **2022**, *14*, 767. [CrossRef]

44. Al-Salahat, M.; Al-Weshah, R.; Al-Omari, S. Dam break risk analysis and flood inundation mapping: A case study of Wadi Al-Arab Dam. *Sustain. Water Resour. Manag.* **2024**, *10*, 74. [CrossRef]

45. Al-Weshah, R.; Tarawneh, A.; Al-Salahat, M. Dam Breach Risk Analysis and Mapping: A Case Study of the Wala Dam, Jordan. *Jordan J. Civ. Eng.* **2025**, *19*, 115–127. [CrossRef]

46. Eldeeb, H.; Mowafy, M.H.; Salem, M.N.; Ibrahim, A. Flood propagation modeling: Case study the Grand Ethiopian Renaissance dam failure. *Alex. Eng. J.* **2023**, *71*, 227–237. [CrossRef]

47. DWR; SDSOD. California Dam Breach Inundation Maps. Available online: https://fmds.water.ca.gov/maps/damim/ (accessed on 6 March 2025).